XIV International Congress of the Mexican Hydrogen Society
Cancun, Mexico, 2014

Synthesis Method Effect of $CoFe_2O_4$ on its Photocatalytic Properties for H_2 Production from Water and Visible Light

Y. Ortega-López[1], J. Salinas Gutiérrez[1], V. Guzmán Velderrain[1],
A. López Ortiz[1], V. Collins Martínez[1*]

[1]Centro de Investigación en Materiales Avanzados S. C., Laboratorio Nacional de Nanotecnología, Depto. de Materiales Nanoestructurados, Miguel de Cervantes 120, C. P. 31109, Chihuahua, Chih. México
. Tel: +52 (614)439 11 29 *e mail: virginia.collins@cimav.edu.mx

ABSTRACT

More efficient materials, which work under the visible light spectrum (energy bandgap from 1.5 to 3.0 eV) are the trends for today's new photocatalysts in the field of hydrogen production. Within this criteria, some transition metal ferrites are ideal. Since, the development of a ferrite-based photocatalytic material will help to address the need for a stable photocatalysts, activated under visible light and with high application potential due to their low cost. In particular, this paper reports cobalt ferrite ($CoFe_2O_4$) as a photocatalyst for hydrogen production, activated under visible light. A comparison between two methods of synthesis; chemical co-precipitation (CP) and milling ball (BM) is presented based on its photocatalytic properties. Furthermore, the influence of the synthesis method over the observed activity is presented. Characterization of $CoFe_2O_4$ was performed by X-ray diffraction (XRD), scanning electron microscopy (SEM), transmission electron microscopy (TEM), BET surface area, UV-Vis spectroscopy and water adsorption/desorption tests. Evaluation of the photocatalytic activity under visible light was followed by gas chromatography. Results indicate that crystalline materials with nanometer sizes were obtained (dp < 25nm). BET areas of 21 and 4 m^2/g and band gap energies of 1.3 eV and 1 eV were found for $CoFe_2O_4$ synthesized by CP and BM techniques, respectively. Water adsorption tests shown an adsorption capacity of 39 for and 30 mg-adsorbed-H_2O/g-catalyst for the CP and BM samples, respectively. The substantial decrease in surface area and adsorption capacity of the ferrite obtained by BM is attributed to a possible sintering process that the material undergoes during its synthesis. Photocatalytic activity results showed better activity for $CoFe_2O_4$ obtained through the BM synthesis. These results are associated with the creation of vacancies in the BM sample that generated a higher water absorption capacity and consequently a greater photocatalytic production of hydrogen.

Keywords: cobalt ferrite, visible light photocatalyst, hydrogen producton.

1. Introduction

Recently, hydrogen has received considerable attention as a next generation energy carrier. While several technologies can be used to generate hydrogen, only some of them can be considered environmentally friendly. There is a general perception that hydrogen is obtained through clean technologies, but this may not be necessarily true. If hydrogen is produced from natural gas (steam reforming), coal or biomass (gasification), a large amount of energy is used, not to mention a substantial amount of CO_2 generated as a byproduct. The latter is the main reason to consider as the best option to produce hydrogen from the splitting of the water molecule, either by using an alternative source of energy like hydraulic, wind or solar. From these alternative energies, solar is the most promising approach, since limitations related to the required space are less demanding.

Hydrogen production via the splitting of the water molecule using solar energy can generally be classified into three types: thermochemical, photobiological and photocatalytic. The principle of the water splitting is thermochemically achieved using concentrators to collect heat from the sun, which can normally reach about 2000 °C and using the collected heat to carry out the dissociation reaction of the water molecule in the presence of a catalyst such as ZnO [1-5]. Although this technique seems to be unsophisticated the management/heat control and the quest for heat resistant materials have become a major challenge. In addition, high concentration solar systems are essential to achieve the requirement of high temperature, which makes this technique often expensive. The photobiological water splitting [6-8], basically can be divided into two groups based on the selected microorganisms, the generated products and the reaction mechanisms involved. Hydrogen production by oxygenic photosynthetic cyanobacteria or green algae under irradiation of light and anaerobic conditions is referred to as water biophotolysis while producing hydrogen for anoxygenic photosynthetic bacteria under light irradiation conditions is known as anaerobic organic biophotolysis. Despite being the water biophotolysis a "clean" way to produce hydrogen than in organic biophotolysis still has several problems waiting to be solved, including low hydrogen yield, enzymes poisoning by the presence of oxygen and the difficulty in design and scaling of a bioreactor for the process.

Moreover, the photocatalytic splitting of the water molecule is another promising technology to produce "clean" hydrogen. Compared to the thermochemical and photobiological process, this technology has the following advantages: cost of the process is low, the ability to separate the hydrogen and oxygen evolution during the reaction and suitable systems for domestic applications with small reactors, thus providing a huge market potential.

Currently, TiO_2 is the most common and widely photocatalyst studied. This is because of its high stability and photocorrosion resistance, a phenomenon that occurs with most common semiconductor materials that can be used. However, their efficiency is very low and the process is limited to the use of high-energy radiation (UV) sources. Radiation of these characteristics can only be provided from artificial mechanisms with the consequent energy expenditure, because the UV light occupies only 4% of the sunlight, which is a limiting factor for the photocatalytic technology using TiO_2 as catalyst. This process for hydrogen production is unique in the sense that it is generated from solar energy, which would become a large clean and economic path for energy generation. It is in this sense that the search for photocatalysts activated under solar radiation (visible light occupies 43% of the solar spectrum) and highly effective, becomes one of the most important challenges in this technology.

One of the synthetic methods used for the preparation of photocatalysts is the co-precipitation technique, as it helps in obtaining a powder precursor of greater homogeneity, by precipitation of intermediates (typically hydroxides or oxalates), so it is an economical synthesis technique. Another easy access and low cost synthesis method is by mechanical milling, which uses more available raw materials and cheaper than other methods [9, 10]. Mechanical milling processes not only can produce an alloy but also, can cause chemical reactions, besides obtaining nanometric size particles [11].

Ferrites are viable alternative materials to TiO_2 to be used as photocatalysts for hydrogen production, transition metal ferrites have a number of advantages, mainly emphasizing their low cost, effective catalytic activity corrosion resistance and most importantly their wide bandgap into the visible light spectrum [12-14]. The selection of these materials is based on the redox activity and especially their ability to store oxygen in its crystalline lattice. Ferrites have a tendency, when burned under reducing atmospheres to form compounds with oxygen defects, which facilitates the fixation of oxygen in the existing vacancies. Therefore, these materials are an excellent candidates for the production of hydrogen from water, while providing the solar energy needed for the process.

The main objective of this study is to synthesize cobalt ferrites by chemical co-precipitation (CP) and mechanical milling (BM) and to determine the effect of the synthesis method on the ferrite photocatalytic activity towards the production of hydrogen.

2. Experimental

CP $CoFe_2O_4$ spinel was prepared by co-precipitation starting from nitrate precursors and modifying the procedure reported by Xialing and Hu [15]. In this method $(Fe(NO_3)_3 \bullet 9H_2O$ and $Co(NO_3)_2 \bullet 6H_2O$ solutions were added to NaOH as precipitating agent. The obtained precipitate was filtered and washed to remove any sodium residue. Thereafter, the residue was dried and placed in an agate mortar to obtain a fine and homogeneous powder. Nanosized crystalline oxide powder was obtained by exposing this to a moderate heat treatment at 250 °C by 6 hours, followed by 1 h at 350 °C.

For the preparation of CoF_2O_4 BM nanoparticles by the mechanical milling technique, the procedure consisted of mixing metallic Fe and Co_3O_4 as precursors in a molar ratio of 2:1. Once the material was in stoichiometric amounts, this was mixed and exposed to 700 ° C by 4 hours. Subsequently, in order to both obtain the desired spinel phase and to reduce particle size, the sample is subjected to mechanical milling with an effective time of 12 hours. The milling was carried out in a Spex CertiPrep 8000M Mixer/Mill, using a weight ratio of balls (0.7cm) to powder ($B:P_w$) of 10:1. To perform this synthesis a D2 steel vial was manufactured, and a exposed to a heat treatment; this consisted of an austenitizing temperature of 1010 ° C, oil quenching and tempering at a temperature varying from 300-400 ° C.

In order to determine the temperatures to be used during the calcination of the samples thermogravimetric analyses were needed from the powders obtained during each synthesis. This analysis was performed on a TGA Instrument TA Q500, using an initial sample weight of about 14 to 15 mg placed in a platinum crucible and employing a heating rate of 10 °C/min from room temperature to 980 °C under an air flow.

Characterization of the samples was performed by X-ray diffraction (XRD) using a PANalytical X'Pert PRO diffractometer with X'Celerator model detector, scanning electron microscopy (SEM) and transmission (TEM) using a JSM-7401F and a Philips model CM-200 microspcopes, respectively. BET

surface area was determined employing an Autosorb-1 equipment and Uv-Vis spectroscopy on a Perkin Elmer lambda 10 model.

The water vapor adsorption-desorption tests were performed by TGA; this test was performed by heating about 14 to 15 mg of sample at 130 ° C under nitrogen flow for 20 minutes to perform a surface cleaning of the sample and followed by an isotherm at 35 ° C to monitor the water adsorption-desorption behavior of the samples in a TA Instrument Q 500 TGA. Photocatalytic coatings were evaluated by splitting of the water molecule, using a 250W mercurial lamp and adding methanol to the water reactor system as sacrificial agent (2% vol). The reaction was monitored by gas chromatography using a GC Perkin Elmer Clarus 500. The system setup employed for carrying out the photocatalytic evaluation of the materials is presented in Figure 1. This system is composed by a photoreactor, artificial lighting and GC analysis with a PC data collection.

In order to monitor the photocatalytic reaction, samples were taken at regular time intervals using a 1ml syringe for gases through a septum located at the upper section of the photoreactor. A sample under darkness was taken as the initial concentration and then the sampling was took place every hour up to a total of 10 hours of irradiation.

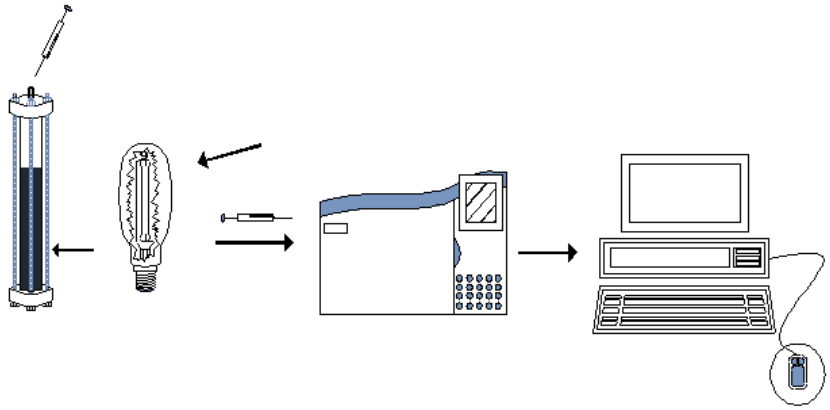

Fig 1. Photocatalytic experimental evaluation setup for the suspension; 0.2 g of $CoFe_2O_4$, H_2O and CH_3OH (sacrificial agent).

3. Results and discussion

3.1. Thermogravimetric Analysis

Determination of the heat treatment temperature of the precipitate product for sample $CoFe_2O_4$ CP during its synthesis was found using a temperature sweep through a thermogravimetric analysis. Figure 2 presents ($CoFe_2O_4$ CP) two signals; both with respect to temperature, one for the weight loss of the sample and the second for the derivative of this. In this Figure it can be observed two slight slope changes at 267 and 350 ° C. In both cases small slopes are observed indicative of slow kinetics. From these data it was considered to establish the temperature and time of heat treatment for this sample, which consisted of keeping the sample for 6 hours at 250 °C and 1 h at 350 °C, this was set in order to achieve the $CoFe_2O_4$ spinel phase, while maintaining a nanometric particle size in the sample, the slower kinetics is compensated by providing a prolonged heat treatment time (6 hours) [16].

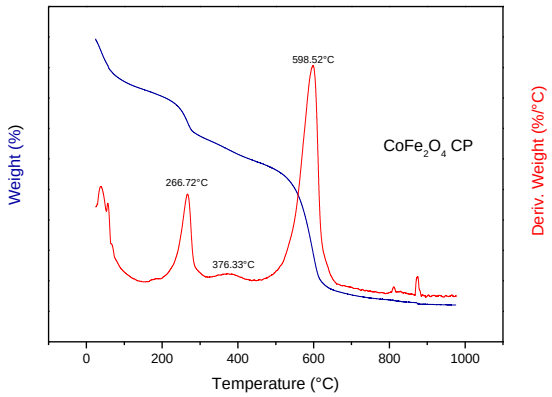

Fig 2. TGA of the precipitate to synthesize $CoFe_2O_4$ CP sample.

In the case of the $CoFe_2O_4$ BM sample determination of the calcination temperature of the Fe and Co_3O_4 mixture was established according to a thermogravimetric analysis. Figure 3 shows the thermogram of the Fe and Co_3O_4 mixture in a stoichiometric ratio ($CoFe_2O_4$ BM), where it is clear that at 700 °C the sample is thermally stable [17]. From the above analysis it was established that the heat treatment was set to 700 °C by 4 hours. Subsequently, the sample was exposed to the mechanical milling process for 12 hours of effective time.

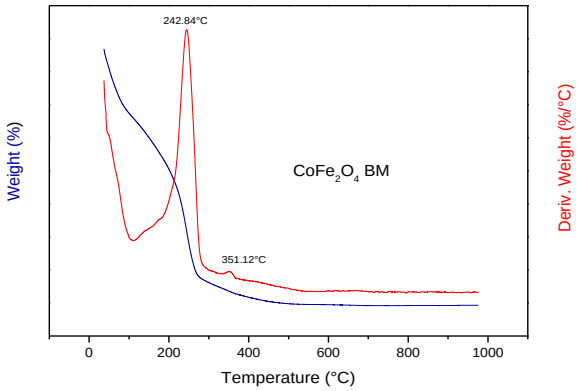

Fig 3. Thermogram for simple $CoFe_2O_4$ BM.

3.2. X-ray diffraction (XRD)

Figure 4 presents the X-ray diffraction pattern for the sample synthesized by chemical co-precipitation, as well as for sample prepared by mechanical milling, $CoFe_2O_4$ CP and $CoFe_2O_4$ BM, respectively. For the data processing, after the proper conversion formats, programs from the Diffrac-Plus package (Bruker AX Systems) were used, including the "Search/Match" identification tool, using the PDF-2 database (ICDD, 2002) ICDD PDF-2 on CD-ROM, Rls 2002, International Centre for Diffraction Data. Pennsylvania, 2002. Analysis of the diffraction patterns indicates that both materials are crystalline, prevailing the $CoFe_2O_4$ spinel phase. However, for the case of the ferrite obtained by chemical co-

precipitation, the Fe_2O_3 phase was also detected, nevertheless that some of the signals from this phase overlap with the $CoFe_2O_4$ phase. This result can be explained considering the phase diagram of Fe-Co-O_2 system (P = atm). For the case of the $CoFe_2O_4$ CP synthesis conditions, which were low temperatures (T < 1400 °C) and stoichiometric ratios of Co and Fe ions; the phase diagram predicts that the solid will consist of a mixture of cobalt ferrite and hematite (Fe_2O_3). While for the sample CoFe2O4 BM, where the initial mixture of metallic Fe and cobalt oxide are exposed to energetic conditions such as high temperature and impact, cobalt spinel is readily possible [18].

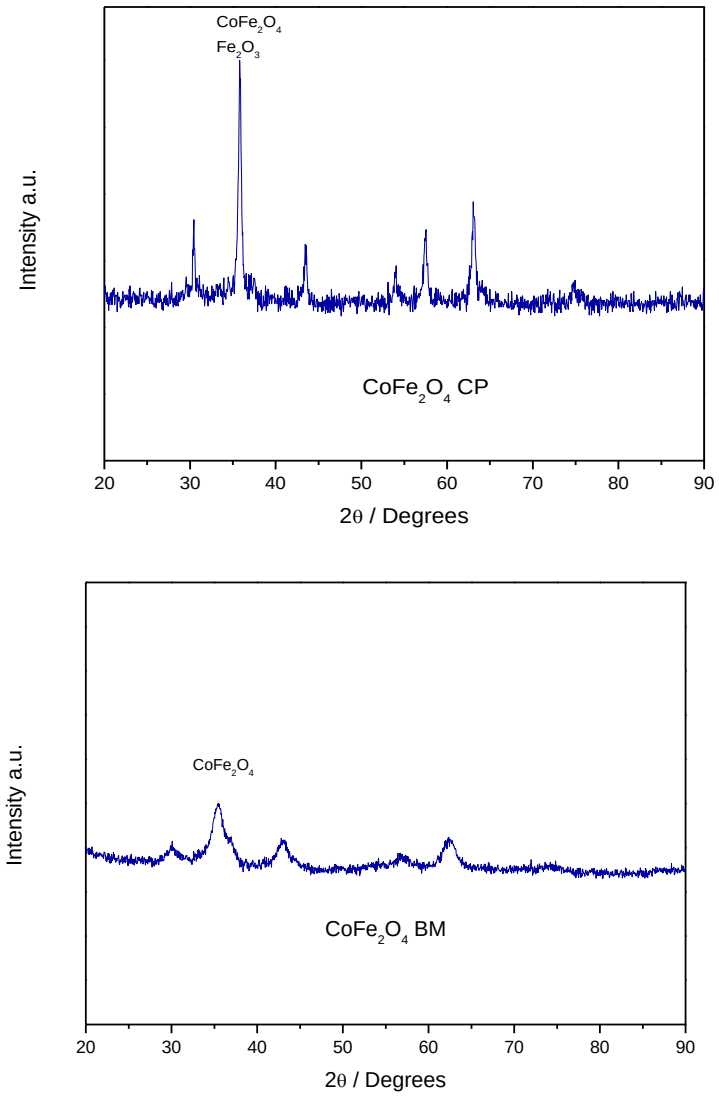

Fig 4. XRD patterns for $CoFe_2O_4$ CP (upper) and $CoFe_2O_4$ BM (lower) samples

Using the information from the X-ray patterns and through the Scherrer equation it was possible to calculate the crystal sizes of the materials. Sample $CoFe_2O_4$ CP present a crystal size of about 20 nm. While, $CoFe_2O_4$ BM sample exhibits a crystal size of around 5 nm, which is extremely smaller than that of

the $CoFe_2O_4$ CP sample. These results are expected, since by comparing the width of the peaks of both diffraction patterns, it can be clearly seen the broadening increase of the XRD peaks for the $CoFe_2O_4$ BM sample, consistent with a decrease of the crystal size, unlike the pattern for the $CoFe_2O_4$ CP sample present narrow and sharp peaks, indicative of a larger crystal size.

3.3. Scanning and Transmission Electron Microscopy

Scanning and transmission electron microscopy were used to determine the morphology and particle size of the samples under study. Figure 5 shows SEM images for samples $CoFe_2O_4$ CP and $CoFe_2O_4$ BM showing that both materials are formed of irregularly shaped agglomerates. Figure 5, CoFe2O4 CP (a) shows the presence of two morphologies. The first is formed by agglomerated nanoparticles, which corresponds to the spinel phase and the second is composed by plate-shaped particles of larger size that corresponds to hematite. These findings were determined according to analyses performed by energy dispersive spectroscopy (EDS), not shown in this work, which in turn confirms the results previously obtained by XRD. While sample $CoFe_2O_4$ BM (b) is formed by large agglomerates, which are composed of particles presenting clear evidence of sintering, which is attributed to the high temperature employed during the synthesis process (700 ° C).

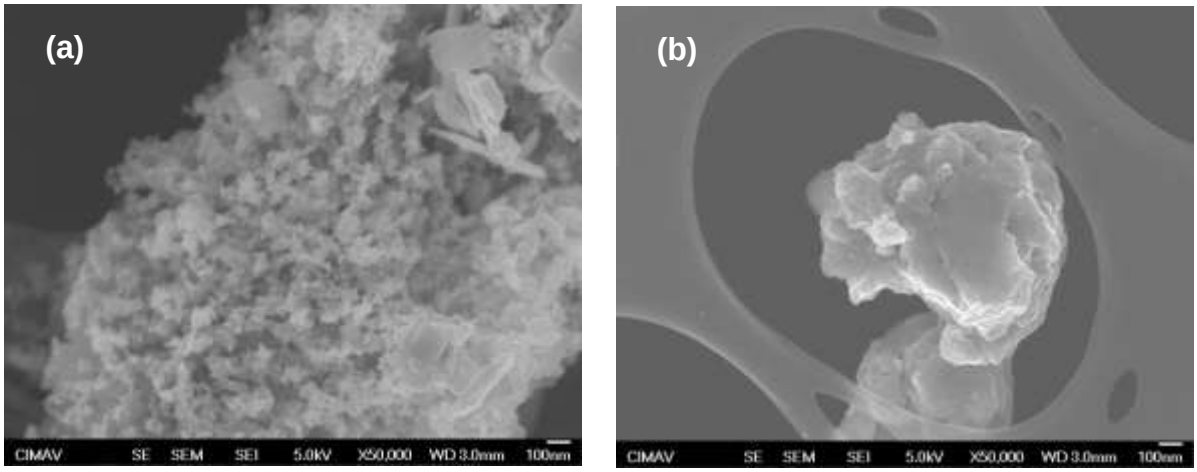

Fig 5. SEM from samples $CoFe_2O_4$ CP (a) and $CoFe_2O_4$ BM. (b)

Figure 6 shows TEM images of the synthesized cobalt ferrite samples. By analyzing the image for $CoFe_2O_4$ CP sample a particle size of around 25 nm can be estimated. This behavior can be associated with the control of the precipitate formation during the synthesis process, which is achieved by strict regulating the flow of the precursor's solutions (both of Co and Fe). Controlled flow induces a slow kinetics behavior for particle nucleation and growth, which makes particles to reach only nanometer sizes. Comparing the above results with those reported by Zhenfa Zi, et al. [19] (who also synthesized cobalt ferrite by co-precipitation) it was found that that research, which reported powders with a particle size between 20 and 30 nm showed very similar behavior to sample $CoFe_2O_4$ CP.

Moreover, also in Figure 6 it can be seen that sample $CoFe_2O_4$ BM exhibits highly compact agglomerates, (where the ultrasonic process was not effective to disperse the sample) with sizes between 100 and 500 nm, and these formed by particles of about 20 nm that apparently were joined together. The

formation of these densified agglomerates is associated with the exposure of the material to the synthesis temperature of 700 °C, confirming the results observed by SEM. However, this sample is nanocrystalline (according to results frm XRD) thus, these highly densified agglomerates tend to behave as a particulate material.

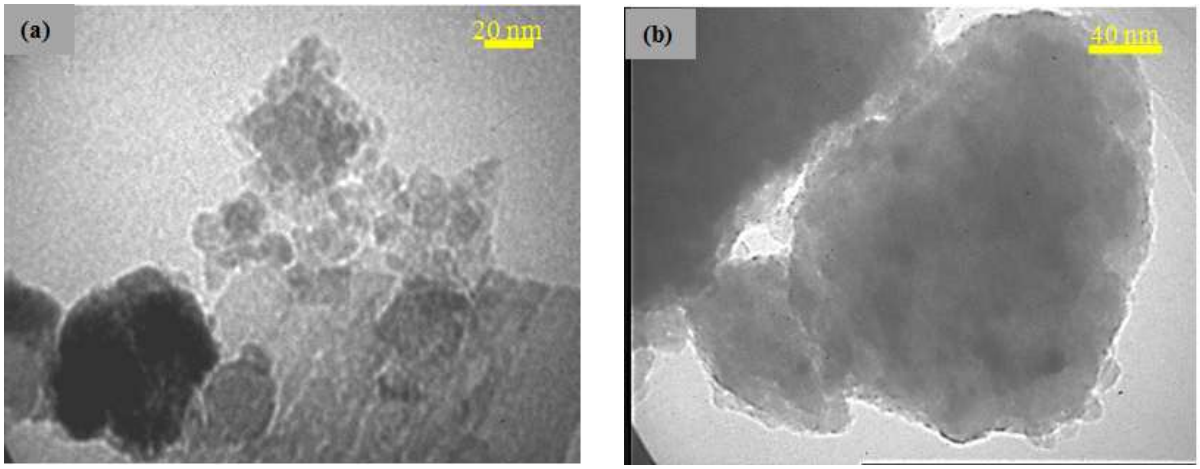

Fig 6. TEM image for samples $CoFe_2O_4$ CP (a) and $CoFe_2O_4$ BM (b).

3.4. BET Surface Area (Brunauer, Emmett y Teller) and Adsorption Isotherms

Values of specific surface areas for the photocatalyst synthesized by chemical co-precipitation and mechanical milling were 20 and 4 m^2/g, respectively. These values can be explained from particle size results determined by transmission electron microscopy.

Sample $CoFe_2O_4$ CP that corresponds to a particle size of 25 nm presented a higher surface area (20 m^2/g) compared to sample $CoFe_2O_4$ BM, which exhibited significantly large particles (agglomerates), ranging from 100-500 nm, which results in a surface area of only 4 m^2/g. The decreasing trend in the specific surface area of materials subjected to mechanical milling can be attributed to a strong aggregation between particles promoted by intensive milling, as reported by Cedeno et al [20].

Figure 7 shows adsorption isotherms for samples $CoFe_2O_4$ CP and $CoFe_2O_4$ BM, where it can be seen that both samples show no hysteresis, suggesting that these samples are non-porous solids. These results are expected since mechanical milling and co-precipitation synthesis methods generally produce non-porous materials.

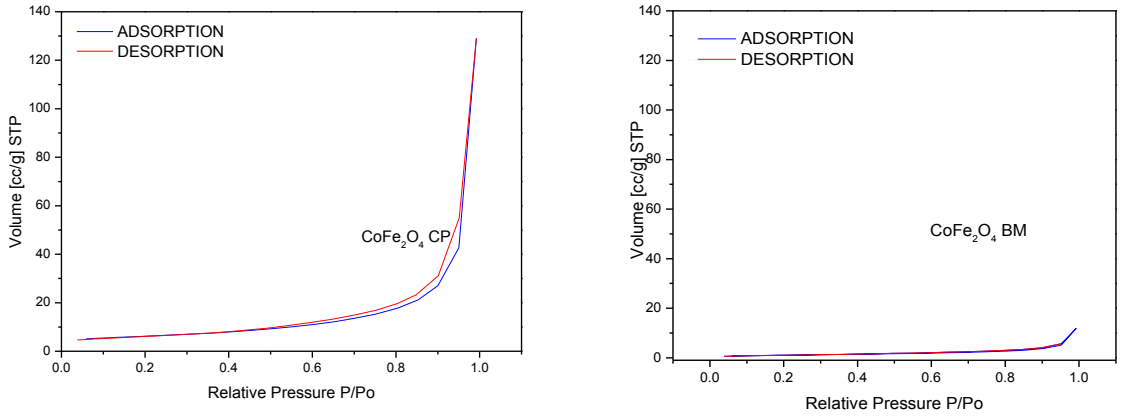

Fig 7. N_2 Adsorption Isotherms for $CoFe_2O_4$ CP and $CoFe_2O_4$ BM samples.

3.5. UV/Vis Spectroscopy

Figure 8 presents the diffuse reflectance UV/Vis spectra for samples $CoFe_2O_4$ CP and $CoFe_2O_4$ BM for an indirect transition employing the Tauc model. These spectra clearly show that values of the energy of the forbidden band are within the visible light spectrum for both cases. The reflectance values were converted in terms of absorption through the Kubelka-Munk function (F(R)) to determine the forbidden bandwidth by extrapolating the linear portion to the abscissa. Obtaining band gap energy value of 1.38 eV for $CoFe_2O_4$ CP and 1.15 eV for $CoFe_2O_4$ BM. Authors like Limei et al. [20] reported very similar values (~ 1.5 eV) to those obtained experimentally. This behavior can be explained with findings reported by Chavan et al, [21], who found that the band gap is highly dependent on the particle size; as the particle size of a ferrite type semiconductor increases its forbidden band decreases and vice versa. Therefore, by comparing the band gap values between the studied samples, it is expected that the $CoFe_2O_4$ CP sample to presents a greater band gap (1.38 eV) than sample $CoFe_2O_4$ BM (1.15 eV). This is because $CoFe_2O_4$ CP is formed by particles of 25 nm size. Whereas, this is opposite for the case of sample $CoFe_2O_4$ BM where the particle size (agglomerates) is significantly higher (100-500nm).

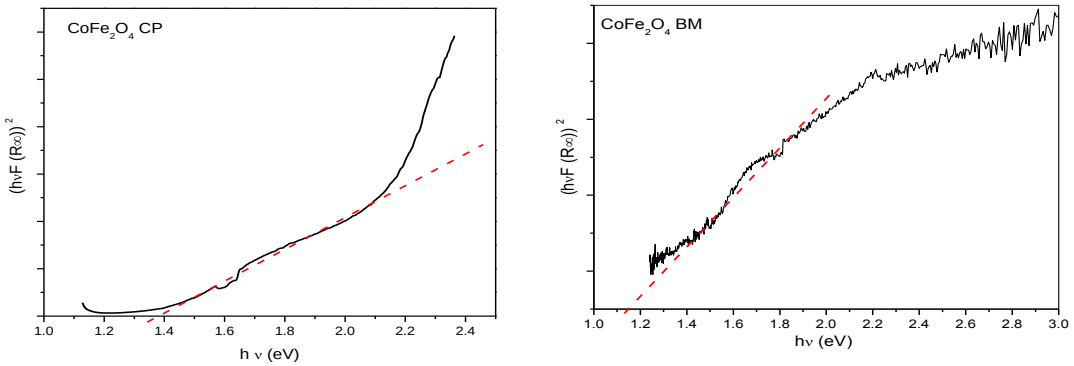

Fig 8. UV/Vis diffuse reflectance spectra (indirect transition model) for $CoFe_2O_4$ CP and $CoFe_2O_4$ BM.

3.6. Water Adsorption and Desorption (Gravimetric Method)

Figure 9 shows graphs of water adsorption-desorption gravimetric isotherms of the synthesized materials. Comparing the water adsorption-desorption capacities of both materials it can be observed that there is a significant difference between the $CoFe_2O_4$ CP sample and the sample one synthesized by mechanical milling (BM $CoFe_2O_4$).

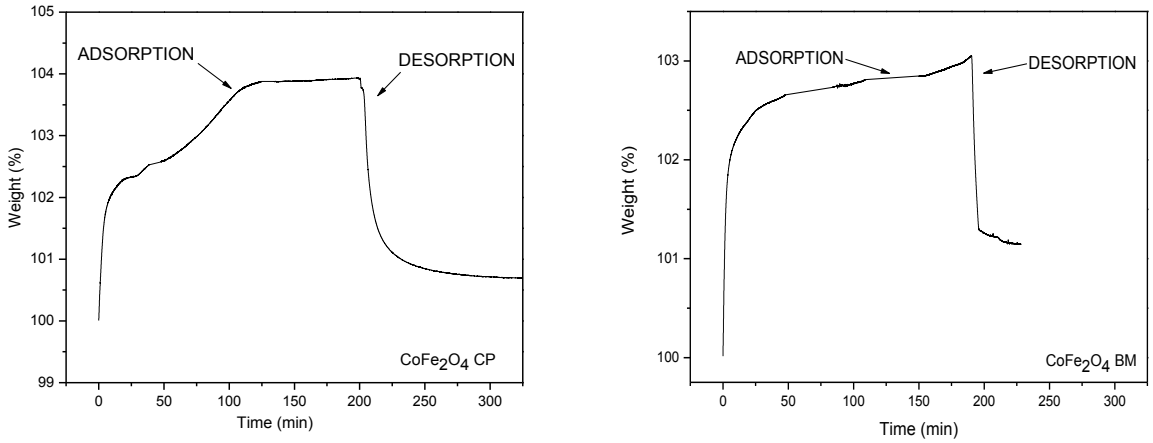

Fig 9. Thermogravimetric analysis for the adsorption-desorption of H_2O for samples $CoFe_2O_4$ CP (left) and $CoFe_2O_4$ BM (right).

Figure 9 shows a thermogravimetric isotherm plot for the adsorption-desorption of water of synthesized $CoFe_2O_4$ CP. Comparing the capacities of both materials, sample $CoFe_2O_4$ CP presented around the double H_2O adsorption-desorption capacity with respect to sample $CoFe_2O_4$ BM (not shown in Figure 9) synthesized by mechanical milling. The water adsorption from the sample synthesized by co-precipitation was about 39 mgH_2O/g, while the sample obtained by mechanical milling had 30 mgH_2O/g. These results are interesting in the sense that if a comparison is made in terms of water adsorption per surface area, it results in a greater water adsorption capacity of the sample synthesized by mechanical milling with 7.5 mg H_2O/m^2 compared to 1.95 mg H_2O/m^2 of sample synthesized by coprecipitation. This behavior can be explained in terms of the activity per unit surface area of each photocatalyst and may indicate that sample $CoFe_2O_4$ BM is photocatalytically more active than CP $CoFe_2O_4$, if a greater water adsorption is associated with an increased formation of OH radicals on the surface of the photocatalyst during the process of formation of the electron-hole pair.

3.7. Photocatalytic evaluation

Figure 10 shows results of the photocatalytic evaluation after 8 hours of irradiation for the samples under study. In this Figure the hydrogen evolution in µmol g^{-1} versus time in h is plotted. An analysis of this figure indicates that the photocatalytic activity towards hydrogen production after 8 hours of irradiation for sample $CoFe_2O_4$ CP exhibited about 2540 µmol g^{-1}, whereas the activity for sample $CoFe_2O_4$ BM was 3490 µmol g^{-1}.

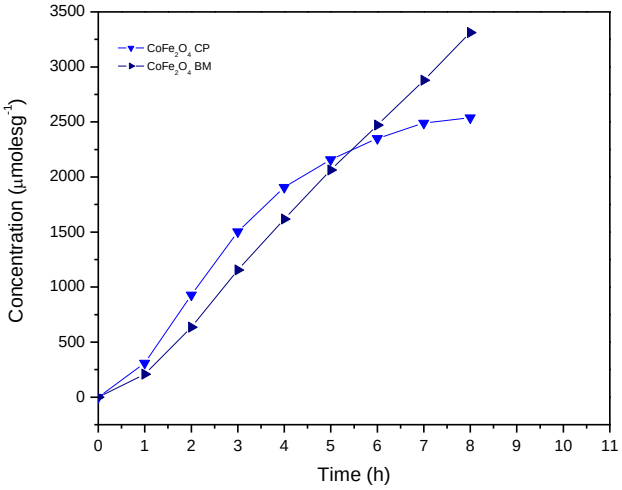

Fig 10. H_2 production after 8 hours of irradiation de H_2 for samples $CoFe_2O_4$ CP and $CoFe_2O_4$ BM

Although both samples can be activated under visible light, photoactivity results can be explained in terms of the morphological, textural, chemical and surface properties that each synthesis method generate on these ferrites. It is important to address that even though some studies are reported for the photocatalytic degradation of contaminants and dyes, so far no studies have been reported using $CoFe_2O_4$ for the production of hydrogen, which makes the activity of this material a significant finding [24,25].

Moreover, the superior photocatalytic activity for sample $CoFe_2O_4$ BM compared to $CoFe_2O_4$ CP can be explained by the findings of Zhang and Geng [26, 27] who reported that the mechanical milling causes a significant increase of vacancies in the solid sample, thus as the density of the vacancies due to collisions increase and these in turn brings about a material that is capable to increase its water adsorption (as reported above) and consequently able to produce a greater amount of hydrogen [28].

4. Summary and perspectives

Cobalt ferrite was successfully synthesized through two different techniques ($CoFe_2O_4$ CP and $CoFe_2O_4$ BM), one by chemical co-precipitation and the other by mechanical milling. These materials presented a band gap energy within the visible range, 1.38 and 1.15 eV, respectively and both exhibiting photocatalytic activity towards hydrogen production. However, sample $CoFe_2O_4$ BM has better photocatalytic activity compared to $CoFe_2O_4$ CP, which is explained by the generation of vacancies present due to hard collisions that occur during the ball milling process, which results in a better photocatalytic activity (3490 µmol g^{-1}) than that obtained through chemical coprecipitation in sample $CoFe_2O_4$ CP (2540 µmol g^{-1}). Even though cobalt ferrite has been used in studies for the photocatalytic degradation of organic pollutants, up to date no studies has been reported the use of $CoFe_2O_4$ for the production of hydrogen under visible light irradiation, which makes the activity found for this material a significant finding.

Acknowledgements

The authors wish to thank to the laboratories of X-ray diffraction, scanning electron microscopy, transmission electron microscopy and catalysis for their help during the progress of the present research.

Our sincere thanks to the Research Center for Advanced Materials (CIMAV) and to the National Council for Science and Technology (CONACYT) for the financial support granted.

References

[1] A. Steinfeld. Solar hydrogen production via a two-step water-splitting thermochemical cycle based on Zn/ZnO redox reactions. Int J Hydrog Energy 2002: 27; 611-619.

[2] R. Fernández-Saavedra, M.B. Gómez-Mancebo, C. Caravaca, M. Sánchez, A.J. Quejido, A. Vidal. Hydrogen production by two-step thermochemical cycles based on commercial nickel ferrite: Kinetic and study. Int J Hydrog Energy 2014: 39; 6819-6826.

[3] A.H. McDaniel, A. Ambrosini, E.N. Coker, J.E. Miller, W.C. Chueh, R. O'Hayre, J. Tong. Nonstoichiometric perovskite oxides for solar thermochemical H_2 and CO production. Energy Procedia 2014: 49; 2009-2018.

[4] F. Fresno, R. Fernández-Saavedra, M. Belén Gómez-Mancebo, A. Vidal, M. Sánchez, M.I. Rucandio, A.J. Quejido, M. Romero. Solar hydrogen production by two-step thermochemical cycles: Evaluation of the activity of commercial ferrites. Int J Hydrog Energy 2009: 34; 2918-2924.

[5] N. Gokon, H. Murayama, A. Nagasaki, T. Kodama. Thermochemical two-step water splitting cycles by monoclinic ZrO_2-supported $NiFe_2O_4$ and Fe_3O_4 powders and ceramic foam devices. Solar Energy 2009: 83; 4 527-537.

[6] I. Akkerman, M. Janssen, J Rocha, R.H. Wijffels. Photobiological hydrogen production: photochemical efficiency and bioreactor design. Int J Hydrog Energy 2002: 27; 1195-1208.

[7] E. Eroglu, A. Melis. Photobiological hydrogen production: Recent advances and state of the art. Bioresource Techn 2011: 102; 18 8403-8413.

[8] I. Akkerman, M. Janssen, J. Rocha, R.H. Wijffels. Photobiological hydrogen production: photochemical efficiency and bioreactor design. Int J Hydrog Energy 2002: 27; 11-12 1195-1208.

[9] O. Kubo, T. Ido, H. Yokoyama. Properties of Ba ferrite particles for perpendicular magnetic recording media. IEEE transactions on magnetics 1982: 28; 6 1122-1124.

[10] R.Valenzuela. Capítulo Preparation of magnetic ceramics. Magnetic Ceramicas. Cambridge 1994: 44-97.

[11] V. Hays. Nanocrystalline Fe-Ni solid solutions prepared by mechanical alloying. Nanostructured Mater 1996: 7; 4 411-420.

[12] N.M. Deraz. Production and characterization of pure and doped copper ferrite nanoparticles. J Anal Appl Pyrol 2008: 82; 212-222.

[13] Y. Haihua, Y Jianhui, L Zhouguang, C Xiang, T Yougen. Photocatalytic activity evaluation of tetragonal $CuFe_2O_4$ nanoparticles for the H_2 evolution under visible light irradiation. J Alloy Compd 2009: 476; 715-719.

[14] A. Kezzim, N. Nasrallah, A. Abdi, M. Tari. Visible light induced hydrogen on the novel hetero-system $CuFe_2O_4/TiO_2$. Energ Conver Manag 2011: 52; 8-9 2800-2806.

[15] X. Hu, P. Guan and X. Yan. Hydrothermal synthesis of nano-meter microporous zinc ferrite. China Particuology 2004: 2; 3 135-137.

[16] D. Nagehan, M. Vedat Akdeniz, O.M. Amdulla. Magnetic monitoring approach to nanocrystallization kinetics in Fe-based bulk amorphous alloy. Intermetallics 2013: 43: 152-161.

[17] A.M. Hamid, A. Abolghasem. Investigation on phase evolution in the processing of nano-crystalline cobalt ferrite by solid-state reaction route. Materials Research 2014: 829: 767-771.

[18] M. Ristic´, B. Hannoyer, S. Popovic´, S. Music´, N. Bajraktaraj. Ferritization of copper ions in the Cu-Fe-O system. Mater Sci Eng B 2000: 77: 73-82.

[19] Z. Zi, Y. Sun, X. Zhu, Z. Yang, J. Dai, W. Song. Synthesis and magnetic properties of $CoFe_2O_4$ ferrite nanoparticles. J Magn Magn Mater 2009: 321: 1251-1255.

[20] Y. Cedeño-Mattei, O. Perales-Pérez, O.NC. Uwakweh. Effect of high-energy ball milling time on structural and magnetic properties of nanocrystalline cobalt ferrite powders J Magn Magn Mater 2013: 341; 17-24.

[21] X. Limei, F. Zhang, C. Bin, X.B. Chen, X. Bai. Preparation of Light-Driven Spinel Nanoparticles $CoAl_2O_4$, $MgFe_2O_4$ and $CoFe_2O_4$ and Their Photocatalytic Reduction of Carbon Dioxide. 2011: ISBN: 978-0-7695-4350-5.

[22] S.M. Chavana, M.K. Babrekarc, S.S. Moreb, K.M. Jadhav. Structural and optical properties of nanocrystalline Ni-Zn ferrite thin films. J Alloy Compd 2010: 507; 21-25.

[23] P. T, Araújo dos Santos, P. T, Araújo dos Santos, A. C. Figueiredo Melo Costa, The Influence Of Calcination Temperature In Ni-Zn Ferrite Doped With Al^{3+}, Proceedings of 21st International Congress of Mechanical Engineering (COBEM 2011), October 24-28, 2011, Natal, RN, Brazil

[24] E. Casbeer, V.K. Sharma, L. Xiang-Zhong. Review: Synthesis and photocatalytic activity of ferrites under visible light. Sep Purif Technol 2012: 87: 1-14.

[25] P.H. Borse, C.R. Cho, K.T. Lim, Y.J. Lee, T.E. Hong, J.S. Bae, E.D. Jeong, H.J. Kim and H.G. Kim. Synthesis of Barium Ferrite for Visible Light Photocatalysis Applications. J of the Korean Physical Society 2011: 58; 6 1672-1676.

[26] B.Q. Zhang, L. Lu, M.O. Lai. Evolution of vacancy densities in powder particles during mechanical milling Physica B 2003: 325; 120-129.

[27] Y. Geng, T. Ablekim, P. Mukherjee, M. Weber, K. Lynn, J.E. Shield. High-energy mechanical milling-induced crystallization in Fe32Ni52Zr3B13 Journal of Non-Crystalline Solids 2014: 404; 140-144.

[28] T. Xia, Y. Zhang, J. Murowchick, X. Che n. Vacuum-treated titanium dioxide nanocrystals: Optical properties, surface disorder, oxygen vacancy, and photocatalytic activities, Catalysis Today 2014: 225; 2-9.

Sociedad Mexicana del Hidrógeno A. C.
Mexican Hydrogen Society

CONACYT

ITC